The Journal of Physiology



# Intrinsic threshold plasticity: cholinergic activation and role in the neuronal recognition of incomplete input patterns

Tuan Pham[1] and Christian Hansel[1,2]

[1] *Committee on Computational Neuroscience, University of Chicago, Chicago, IL, USA*
[2] *Department of Neurobiology, University of Chicago, Chicago, IL, USA*

Handling Editors: Katalin Toth & Michael Okun

The peer review history is available in the Supporting Information section of this article (https://doi.org/10.1113/JP283473#support-information-section).

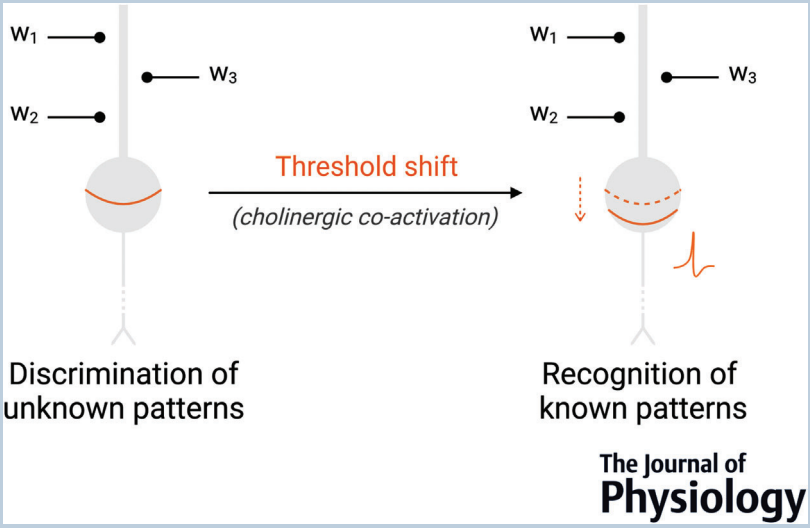


**Abstract** Activity-dependent changes in membrane excitability are observed in neurons across brain areas and represent a cell-autonomous form of plasticity (intrinsic plasticity; IP) that in itself does not involve alterations in synaptic strength (synaptic plasticity; SP). Non-homeostatic IP may play an essential role in learning, e.g. by changing the action potential threshold near the soma. A computational problem, however, arises from the implication that such amplification does not discriminate between synaptic inputs and therefore may reduce the resolution of input representation. Here, we investigate consequences of IP for the performance of an artificial neural network in (a) the discrimination of unknown input patterns and (b) the recognition of known/learned patterns. While negative changes in threshold potentials in the output layer indeed

**Tuan Pham** earned his Bachelor of Arts degree in Behavioural Neuroscience from Lehigh University in 2018, working on electrical synapse modelling with Dr Julie Haas in the Department of Biological Sciences. He received his Master of Science degree in Computational Neuroscience from the University of Chicago in 2021, working with Dr Christian Hansel in the Department of Neurobiology. In Chicago, his work focused on the potential effects of intrinsic plasticity on neural information processing using computational modelling.

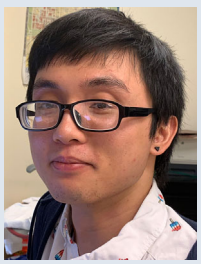



DOI: 10.1113/JP283473

reduce its ability to discriminate patterns, they benefit the recognition of known but incompletely presented patterns. An analysis of thresholds and IP-induced threshold changes in published sets of physiological data obtained from whole-cell patch-clamp recordings from L2/3 pyramidal neurons in (a) the primary visual cortex (V1) of awake macaques and (b) the primary somatosensory cortex (S1) of mice *in vitro*, respectively, reveals a difference between resting and threshold potentials of ∼15 mV for V1 and ∼25 mV for S1, and a total plasticity range of ∼10 mV (S1). The most efficient activity pattern to lower threshold is paired cholinergic and electric activation. Our findings show that threshold reduction promotes a shift in neural coding strategies from accurate faithful representation to interpretative assignment of input patterns to learned object categories.

(Resubmitted 15 June 2022; accepted after revision 15 July 2022; first published online 25 July 2022)
**Corresponding author** C. Hansel: University of Chicago, Department of Neurobiology, 947 E. 58th Street/J243, Chicago, IL 60637, USA. Email: chansel@bsd.uchicago.edu

**Abstract figure legend** A neuron with a given synaptic input distribution (left) that has a high spike threshold (curved orange line) will perform well in an object discrimination task. Lowering the spike threshold upon threshold plasticity induced by cholinergic co-activation will enhance the probability of spike output even when only some inputs are active (right). This computational mode is beneficial for the recognition/detection of known patterns, even when details are missing or only details are presented.

**Key points**

- Intrinsic plasticity may change the action potential threshold near the soma of neurons (threshold plasticity), thus altering the input–output function for all synaptic inputs 'upstream' of the plasticity location.
- A potential problem arising from this shared amplification is that it may reduce the ability to discriminate between different input patterns.
- Here, we assess the performance of an artificial neural network in the discrimination of unknown input patterns as well as the recognition of known patterns subsequent to changes in the spike threshold.
- We observe that negative changes in threshold potentials do reduce discrimination performance, but at the same time improve performance in an object recognition task, in particular when patterns are incompletely presented.
- Analysis of whole-cell patch-clamp recordings from pyramidal neurons in the primary somatosensory cortex (S1) of mice reveals that negative threshold changes preferentially result from electric stimulation of neurons paired with the activation of muscarinic acetylcholine receptors.

## Introduction

Synaptic plasticity, and in particular long-term potentiation (LTP; Bliss & Lomo, 1973; Nabavi et al., 2014), is widely considered as the primary cellular correlate of learning. The synaptic theory of learning has been challenged, however, based on the observation that properties of behavioural learning, such as the duration of the learning phase or learned time intervals, do not match properties of synaptic plasticity (see Gallistel & Balsam, 2014; Gallistel & Matzel, 2013). Cell-autonomous forms of plasticity, intrinsic to activated cells, have emerged as alternative learning correlates (Gershman et al., 2021) that may replace (Gallistel, 2017; Johansson 2019; Johansson et al., 2015) or critically complement (e.g. Hansel & Disterhoft 2020; Josselyn & Tonegawa 2020; Titley et al., 2017) synaptic plasticity in its role in learning. Cell-autonomous plasticity may rest on prolonged changes in membrane excitability and spike firing properties (Hansel et al., 2001; Marder et al., 1996), and this type of plasticity ('intrinsic plasticity'; IP) is considered here. Note, however, that cell-autonomous plasticity is not restricted to changes in excitability, and that excitability changes – when they occur – can also be homeostatic in nature (Turrigiano, 1999). IP has been observed in response to activity patterns or in the context of behavioural learning both *in vitro* and *in vivo*, in types of neurons as diverse as cortical pyramidal neurons (e.g. Mahon & Charpier, 2012; Moyer et al., 1996;

Paz et al., 2009) and cerebellar Purkinje cells (e.g. Belmeguenai et al., 2010; Schreurs et al., 1998; Titley et al., 2020).

Computationally, the role of IP (including homeostatic IP) may be to adjust the membrane threshold and excitability to an optimal target rate (Del Papa et al., 2019; Lazar et al., 2007; Li et al., 2018; Loidolt et al., 2020; Naude et al., 2013; Wu et al., 2020; Zheng & Triesch, 2014), or it may be to alter the excitability set-point to maximize information transfer between synaptic inputs and spike output (Joshi & Triesch, 2009; Li & Li, 2016; Li & Li 2013; Savin et al., 2010; Shaw et al., 2020; Stemmler & Koch, 1999; Triesch, 2005, 2007; Zhang & Li, 2019; Zhang et al., 2019). IP models have been used to explain homeostasis (LeMasson et al., 1993; Marder & Prinz, 2002; Wu et al., 2020), sequence learning (Loidolt et al., 2020), networks with rich dynamics (Naude et al., 2013; Zheng & Triesch, 2014), criticality of neural networks (Del Papa et al., 2019; Naude et al., 2013) as well as receptive field development (Savin et al., 2010; Triesch, 2005, 2007). At the same time, their application has been explored in reservoir computing for classification and regression tasks (Steil, 2007; Wang et al., 2020), as well as more recently in machine learning algorithms (Shaw et al., 2020; Zhang & Li, 2019; Zhang et al., 2019) and neuromorphic computing implementation (Baek et al., 2020; Dalgaty et al., 2019). In contrast to these implications, the role of IP in the encoding of input patterns, e.g. in object recognition in sensory physiology, but also in more abstract pattern encoding in general, remains underexplored in computational biology. This is despite the fact that threshold setting is a well-known problem (and solution) in the engineering of software for face/object recognition.

In neural networks, the issue at hand is generally the same, but presents itself in a slightly more complex way as individual neurons – via their synaptic input – may receive information about several unrelated objects or patterns. Moreover, network connectivity is not determined by engineering goals, but is set by biological rules during brain development. While principles of cortical connectome development and architecture are known (e.g. Felleman & Van Essen, 1991; Innocenti, 1981, 1995; Izhikevich & Edelman, 2008; Singer, 1995), it is difficult to determine the settings of specific network parameters, such as synaptic weights, input–output selectivity, or neuronal excitability. A phenomenon that is shared, though, is that a threshold reduction at the output stage (in biological neurons, IP is triggered at or near the soma) facilitates activation, but may reduce the resolution of input representation, thus enhancing 'graininess'. In a biological neuron, enhanced excitability via IP results in an amplification that does not differentiate between synaptic inputs 'upstream' of the location that experienced the increase in excitability. The consequences of this phenomenon for perception and signal encoding in neural networks have not been studied so far. Hence, we set out to investigate the consequences of IP for the detection and differentiation of unknown input patterns as well as the recognition of known or learned patterns. There are different physiological aspects of IP, including changes in the spike threshold, in excitability as measured by the number of evoked spikes, or the amplitude of the afterhyperpolarization (AHP) that may follow spike bursts. Our study focuses on the spike threshold as the only IP parameter that by definition separates 'non-spike' from 'spike' states, which determine whether information encoded by a neuron is further conveyed through the network.

Here the term 'pattern' is used to describe general input patterns, which may be any pattern of information that is conveyed via synapses onto neurons. However, for illustrative purposes we will use examples from object recognition in sensory physiology. Indeed, the inspiration for the recognition task comes from a simplified analogy to face recognition – of both individual faces and 'face' as an object category – posed by Titley et al. (2017) when discussing the problem of neuronal activation and integration into ensembles, in situations where fine-scale object details are missing, or only local structural inputs are presented. With the neural code (portfolio of information that is represented) of concept cells set up by synaptic connectivity patterns, enhancing intrinsic excitability through IP would amplify the ultimate responsiveness of the neuron to all its inputs without differentiation. This could result in a more robust representation (and possibly categorization) of the concept (e.g. a face) of interest, when its inputs lack certain details. Moreover, such effects of categorization by design can be obtained by regulating intrinsic amplification alone, without the need for changing synaptic weights, which might come at the cost of changing synaptic weight ratios and thus possibly the information content that is represented.

Here we perform a parametric study on a two-layer feedforward network consisting of inputs selective for certain binary output units. Our main goal is to determine consequences of threshold change for network performance in two tasks: (a) a pattern distinction task, in which IP is expected to lower performance and (b) a recognition task for reporting already known or learned patterns. In contrast to similar computations used in software engineering applications, our study introduces ambiguities inherent to biological or biologically inspired artificial neural networks that arise from unknown connectivity parameters: selectivity of the output units (neurons) for input features, and selectivity in the presentation of such features by the input units. The main result of our study is that a decrease in output threshold may facilitate pattern recognition, in particular when

inputs are incomplete and network selectivity is imperfect. This finding demonstrates that IP – in form of a negative threshold shift – is beneficial under conditions when neurons have to interpret incomplete input patterns and assign them to a specific pattern or object category. In addition, we re-analyse published data sets obtained during whole-cell patch-clamp recordings from L2/3 pyramidal neurons in cortex to determine physiological threshold ranges. We identify electrical activation paired with cholinergic signalling as an activity pattern that promotes a lasting negative threshold change and thus drives neurons into a signalling mode that favours the detection of known input patterns.

## Methods

### Discrimination of input patterns in a two-layer feedforward network

The model used consists of a two-layer feedforward network with $N_X$ (usually 10) number of input $X$ units and $N_Y$ number of binary output $Y$ units. They are connected via the weight matrix $W$, first initialized from a uniform distribution $U[0, 1]$, then normalized to a sum of 1 for each $Y$ (L1 normalization). In other words, the entries in $W$ are constructed as $W_{Y_j,X} = U'(N_X) \forall j \in [1, N_Y]$ eqn (1).

$$U'(N) = \left\{ \frac{w_i}{\sum_i w_i} \right\} \text{ where } w_i \sim U[0, 1] \text{ for } i \in [1, N] \tag{1}$$

The output activity $Y_j$ is binary, characterized by a Heaviside activation function, with a threshold $\theta_j$ eqn (2). Decreased thresholds are synonymous with increased neural intrinsic excitability. Initially, these thresholds are parameterized and sampled from $U[0, 1]$.

$$Y_j = H(W_{Y_jX}X \mid \theta_j) = 1 \text{ if } \sum_i W_{ji}X_i > \theta_j \text{ or } 0 \text{ otherwise} \tag{2}$$

When presenting all possible binary input patterns, we quantify the entropy of the output patterns eqn (3) as a function of $W, \theta$, along with the number of unique output patterns to present a measure of discriminability at the output layer. We also optimize such measure at baseline (i.e. $\Delta\theta = 0$) and then observe the effects of output threshold changes on performance in the discrimination task.

$$S(Y) = -\sum_j P\left(\sigma_Y^{(j)}\right) \log_2 P\left(\sigma_Y^{(j)}\right) \text{ where } P\left(\sigma_Y^{(j)}\right) \text{ is the probability of the output state } \sigma_Y^{(j)} \in \{0, 1\}^{N_Y} \tag{3}$$

We choose a simple approach to optimize the Euclidean distance with a randomly selected output pattern set. For each network instantiation, a random mapping between $2^{N_X}$ input patterns ($\sigma_X^{(j)} \in \{0, 1\}^{N_X}$) and output patterns ($\sigma_{Y'}^{(j)} \in \{0, 1\}^{N_Y}$) is chosen to optimize for the Euclidean distance loss eqn (4). We track the entropy of the output patterns along the process and pick the maximum entropy state as our 'best' solution. This approach was selected over other loss function choices, because of its inherent simplicity.

$$L \sim (Y, Y') = \left\langle \left\| Y - Y' \right\|_2 \right\rangle \quad \text{where } Y' \text{ is the desired output state and } \|\bullet\|_2 \text{ is the L2 norm} \tag{4}$$

In addition, for a specific minimally shared input pattern $k$ (for simplicity, assumed for only the first $k$ input units that are always activated), we quantify the resulting mean pairwise output distances (either Jaccard distances $J_d$ in eqn (5) or normalized Hamming distances $H_d$ in eqn (6)) as another measure of discriminability. This is shown in Fig. 1 for the best states, with $N_X = 10$ for different $N_Y$.

$$J_{\mathrm{d}}\left(Y^{(1)}, Y^{(2)}\right) = 1 - \frac{\#\{i | Y_i^{(1)} = Y_i^{(2)} = 1\}}{\#\{j | Y_j^{(1)} = 1 \text{or} Y_j^{(2)} = 1\}} \quad \text{where } \begin{cases} Y^{(1)}, Y^{(2)} \text{ are output vectors} \\ \#\{\bullet\} \text{ is the cardinality of a given set} \end{cases} \tag{5}$$

$$H_{\mathrm{d}}\left(Y^{(1)}, Y^{(2)}\right) = 1 - \frac{\#\{i | Y_i^{(1)} = Y_i^{(2)}\}}{N_Y} \tag{6}$$

Both quantify the number of differences between binary patterns, but $J_{\mathrm{d}}$ is normalized by the total number of activated locations between both patterns, while $H_{\mathrm{d}}$ is normalized by the length of the patterns. Note that this results in $J_{\mathrm{d}}$ being more biased towards activated units, and not being defined when there are no activated units in both patterns (hence the red lines are cut off at the right hand side of the panels in Fig. 1). These simulations were run on the Neuroscience Gateway (Sivagnanam et al., 2013).

### Model to test the effect of threshold changes on the number of inputs needed for suprathreshold activation

To demonstrate that incomplete pattern recognition could benefit from increased excitability, we use a simple binary unit $Y$ receiving inputs from 10 binary $X$ units. For simplicity, we represent the connectivity in the network with an excitatory vector $W$ (Fig. 2*A* and *B* top). The weights are constructed either from a uniform distribution $U[0, 1]$ (Fig. 2*A*) or set equal (Fig. 2*B*), then normalized to a sum of 1. The normalization allows us to control the range of the output threshold. In other words, $W = U'(N_X = 10)$ eqn (1).

The output activity $Y$ is binary, characterized by a Heaviside activation function, with a threshold $\theta \in [0, 1]$ eqn (2). We assume that $Y$ represents an input pattern (such as a complex object or concept) that the downstream network associates with activation of all of these input units. Hence, *incomplete patterns* would be any binary representation of $X$ where at least one unit is 0 (Fig. 2*Aiv* and *Biv*).

## Recognition of known or learned input patterns in a binary two-layer feedforward network

**Overview description.** We use a simple feedforward network with two layers: 150 input units in the $X$ layer and three binary output units in the $Y$ layer (Fig. 3*A*). Each output unit is considered to represent an input pattern. The weight matrix $W_{YX}$ is non-negative, characterized by a selectivity index $\alpha_W$ and selectivity overlap (Fig. 3*B*).

The inputs are generated at $X$, characterized by a percentage completeness to allow for incomplete input patterns, with additive normal-distributed noise (Fig. 3*C*). The outputs at $Y$ are binary, activated by a Heaviside step function with their own thresholds set to a base threshold $\theta_{\text{base}}$ and an additional change $\Delta\theta$ applied to the threshold of only one output neuron (Fig. 3*A*). Otherwise, all neurons in the input layer $X$ and in the output layer $Y$, respectively, are identical (non-parameterized). The task of interest is *recognition* of a known/learned pattern of interest by the tested output unit. The term 'incomplete pattern' in the context of the recognition task refers to a deviation from the known/learned pattern, in which components of the complete pattern are missing.

Note that our model does not contain recurrent network components (Hopfield, 1982). This selection was made as our goal is to isolate emerging consequences of cell-autonomous intrinsic plasticity of neurons, whose output function informs a measure of task performance. It is anticipated that with the recurrent connectivity properties of a Hopfield model (recurrent connectivity within the input layer), output layer activation would differ. However, we expect that the consequences of threshold changes in an output layer neuron for task performance would qualitatively remain the same.

**Selectivity and connectivity.** The 150 inputs in $X$ are selective for either none, only one or all of the outputs in $Y$. The number of inputs selective to each output unit is kept fixed at $N_{\text{selec}} = N_X \,/\, N_Y = 150/3 = 50$.

The non-negative weights in matrix $W_{YX}$ are characterized by the *selectivity index* $\alpha_W \in [0, 1]$ eqn (7) – a higher value means that more weights are concentrated on the corresponding selective output (Fig. 3*B*, left to right). Thus, $\alpha_W$ describes selectivity in responsiveness of the outputs in $Y$.

$$\begin{aligned} W_{Y_jX} &= \{W_{\text{selec}},\ W_{\text{nonselec}}\} \\ \text{where } &\begin{cases} W_{\text{selec}} &= \alpha_W \cdot U'\left(N_{\text{selec}}\right) \\ W_{\text{nonselec}} &= \left(1-\alpha_W\right) \cdot U'\left(N_X - N_{\text{selec}}\right) \end{cases} \end{aligned} \tag{7}$$

Additionally, the weight matrix is also characterized by *selectivity overlap* (overlap in the inputs in $X$). For example, Fig. 3*B* top panels are examples of zero selectivity overlap, while the bottom panels have 20 input units that overlap and are represented by all three outputs. For each parameter set, we run 10 instantiations of $W_{YX}$.

The identity of which output(s) each input is selective for is defined beforehand, and is also influenced by the selectivity overlap parameter but the number of selective inputs per output remains fixed ($N_{\text{selec}} = 50$).

**Input generation.** The inputs at $X$ are generated with binary states (before noise is added) to represent only one pattern in each example. To represent input incompleteness, the parameter *% complete* (Fig. 3*C*) controls the percentage of the inputs that are active. On top of this, there is an additive noise drawn from a zero-mean normal distribution with a fixed width of $\sigma_{\text{noise}} = 0.8$.

**Output activation.** The output units at $Y$ are activated by a Heaviside step function eqn (2), each with their own threshold value. For simplicity, we set all output thresholds to a base threshold $\theta_{\text{base}} = 0.5$, and apply a change only to one output unit with an amplitude of $\Delta\theta \in [-0.5, 0.5]$.

**Task of interest.** For each manipulation of $\Delta\theta$ in a selected output unit, we generate 2000 random input patterns and characterize the outputs at $Y$ to evaluate performance of *recognition* (of known/learned patterns), via the true-positive rate (TPR) of *only* the output whose threshold is changed with $\Delta\theta$. Activity in other output units is disregarded (in other words, all the other outputs would be considered noise or irrelevant; note that if threshold changes in multiple neurons were considered, the error rate is expected to differ). Receiver operating characteristics (ROC; a method to show classification performance, graphically displayed as TPR *vs.* false positive rate (FPR)) analysis for recognition is plotted in Fig. 4*B*.

**Optimal activation threshold change.** For each parameter set and performance curve $f(\Delta\theta)$ of a given task, $\Delta\theta_{\text{optim}}$ is defined as the change of threshold $\Delta\theta$ whose absolute value is the smallest, while resulting in the highest performance outcome. In other words, we define the '*optimal' threshold change* as the change nearest to 0 to

achieve the maximum performance. These are shown in Fig. 4*C* and *D*.

### Measurement of biological resting and threshold potentials

**V1 *in vivo* biological thresholds.** We obtained the *in vivo* resting and threshold potentials of layer 2/3 neurons in V1 from recordings performed in awake macaques (Li et al., 2020) (see summary of data in Fig. 5*A*). We denote membrane thresholds as $V_T$, resting potentials as $V_R$ and the distance between them as $\Delta V_{TR} = V_T - V_R$. The biological data statistics are reported as means ± SD.

**S1 *in vitro* biological thresholds.** We calculate resting and threshold potentials from *in vitro* recordings from mouse S1 L2/3 pyramidal neurons that we published previously (Gill & Hansel, 2020). This data set includes three groups of intrinsic plasticity experiments: (i) *electric group* – electric tetanization using somatic depolarization or synaptic tetanization, (ii) *cholinergic group* – bath application of the agonist of muscarinic acetylcholine receptors (mAChRs) oxotremorine-m (oxo-m), and (iii) *cholinergic paired group* – co-application of oxo-m when electric stimulation is applied. Bath application of an mAChR agonist is intended to activate mAChRs that are primarily located on the extrasynaptic membrane of pyramidal cell dendrites and spines (McCormick & Prince, 1985; Yamasaki et al., 2010). The somatic depolarization protocol in (i) consisted of 10 depolarizing current pulses (50 ms duration) that were delivered at 10 Hz, followed by 2 s of holding current. The depolarization amplitude was adjusted to evoke one to three spikes during each of these pulses and was repeated 100 times for a total duration of 5 min. The synaptic tetanization protocol in (ii) mimicked the overall timing presented in the somatic protocol, but now somatic current injection was replaced by extracellular stimulation using 10 Hz pulses (applied for 1 s) followed by 2 s of no stimulation. This pattern was repeated 100 times. In the co-activation protocol (iii), only somatic depolarization was used. For further experimental details, see Gill & Hansel (2020). Six new recordings were added to increase the statistical power of the analysis presented here. These recordings followed the same protocol as described in Gill & Hansel (2020).

To calculate the resting potentials $V_R$, we use the holding current ($I_{hold}$) and the recorded potential 20 ms before test pulse ($V_{spont}$), along with the input resistance ($R_{in}$): $V_R = V_{spont} - I_{hold}R_{in}$ (assuming zero net active components at rest at steady state). The threshold potential $V_T$ is detected as the potential first crossing 8 V/s (for a similar approach, see Mahon & Charpier, 2012; Popescu et al., 2021) around 1 ms before the *first* action potential. We also look at the difference between resting and threshold potentials $\Delta V_{TR} = V_T - V_R$ to assess intrinsic excitability. The distributions of these data are shown in Fig. 5*B*.

For *baseline* (pre-induction; denote with superscript $x^0$ for a property $x$), we take the average measures (either resting or threshold potentials) of the last four sweeps before application of any plasticity protocol. For *post* measurements (denote as $x^f$), we take at least 10 sweeps near the end of the experiment of each cell for average. Change between pre- and post-induction properties is denoted as $x^\Delta = x^f - x^0$ (Fig. 5*D*). Additionally in this figure panel, linear fits, along with their *P*-values and $R^2$ are shown for functional excitability changes (number of spikes $n^\Delta_{spk}$) related to changes in membrane potential measures ($V^\Delta_R$, $V^\Delta_T$, $\Delta V^\Delta_{TR}$).

In addition, we determined the theoretically conceivable lower and upper threshold bounds which, for illustrative purposes, are shown together with our modelling results in Fig. 5*C*. We define the biological lower bound as the average of all resting potentials in Gill & Hansel (2020), plus new experiments. To define the biological threshold upper bound, we obtained recordings from four additional S1 cells (same recording conditions as in Gill & Hansel, 2020). In these recordings, we evoked multiple action potentials by injecting depolarizing current pulses. We took the threshold potentials measured during the relative refractory state as the upper bound of threshold potentials. This relative refractory state is characterized by a reduction in AP amplitude after the first spike was fired as well as a spike threshold at a more depolarized membrane potential.

**Statistical analysis.** Statistical significance was determined by using the two-sample unpaired Student's *t*-test (between-group comparison; V1 *vs.* S1 cortex) and the paired Student's *t*-test (within-group comparison of baseline *vs.* post-manipulation changes; plasticity experiments), when appropriate. The Pearson correlation coefficient was used to statistically describe correlations between spike output and threshold potential (and related parameters). All statistics are reported as means ± SD. The chi-square test is used to examine the distribution of negative *versus* non-negative threshold shifts in the plasticity experiments.

## Results

### Threshold decrease results in a reduced ability to discriminate distinct input patterns

It is expected that threshold plasticity, when taking place close to the soma and therefore 'downstream' of dendritic input locations, indistinctively amplifies

synaptic responses. This downstream amplification may lead to reduced resolution and thus a decrease in the ability to discriminate input patterns. To quantitatively describe this effect, we modelled a two-layer feedforward network (Fig. 1) and inspected the output discriminability via output pattern distributions and pairwise distance for both random (initial) and optimized states (via Euclidean loss, see Methods).

Across a wide range of values of $N_X$, $N_Y$, we observe that the effects of threshold change in the output layer $\Delta\theta$ on the number of unique output patterns and on output entropy in the random initial states are generally symmetric. The optimization process via minimization of the Euclidean loss for output patterns results in a small decrease in the output thresholds, creating the asymmetry in the peak values of the output entropy and pattern number (as a function of $\Delta\theta$ to shift to the right), especially for small $N_Y$. The $\Delta\theta$ for the peak values in these curves tends towards positive change, exemplifying how decreased thresholds may harm discriminability.

Another way to quantify discriminability is to look at the pairwise distances between the binary output patterns using known distance measures such as the Jaccard distances $J_d$ or the normalized Hamming distances $H_d$ (Fig. 1*B–D*). Instead of observing these distances for all input patterns, we chose a minimal common input activation number $k$, to parameterize input overlap when quantifying output discriminability. The relationship

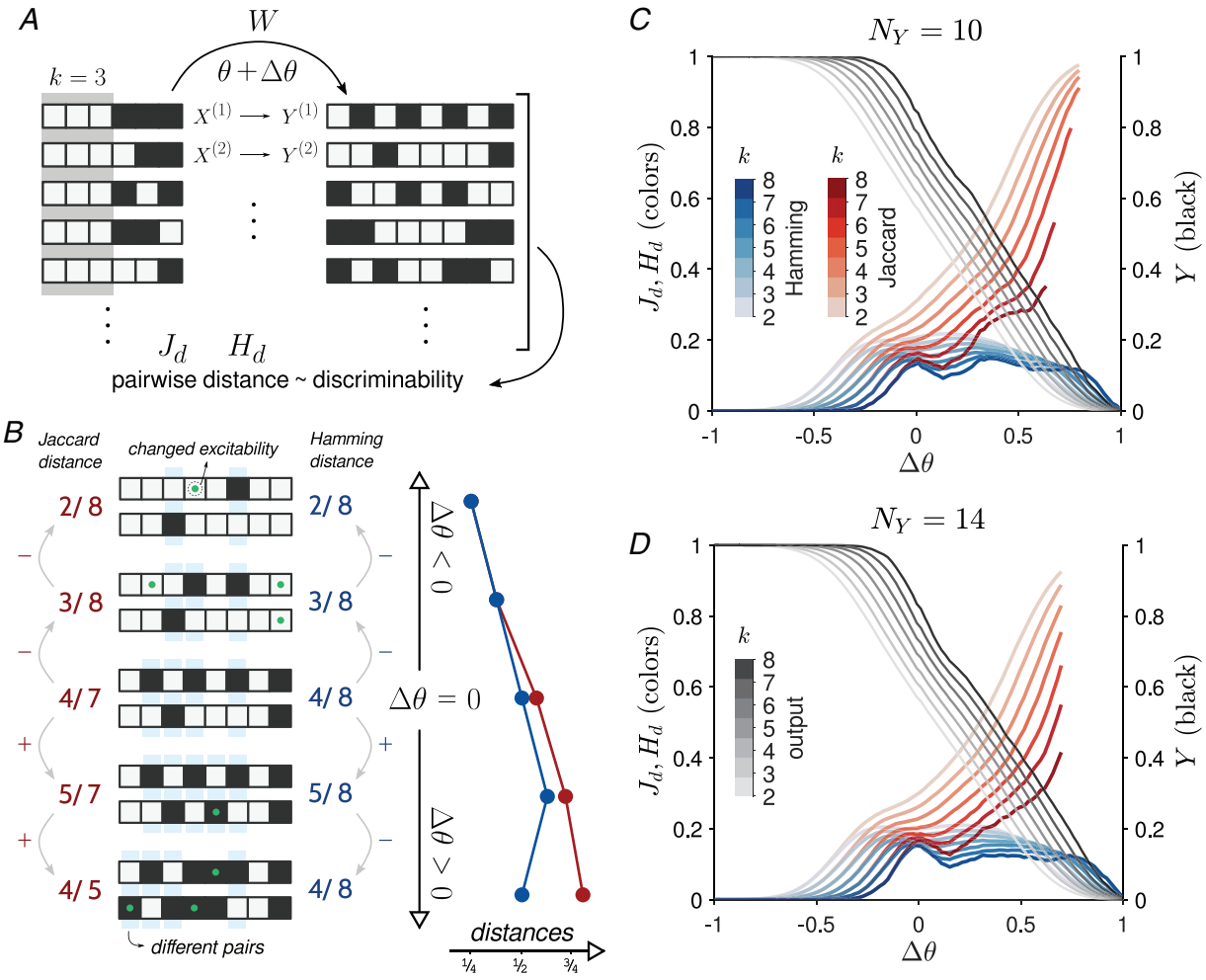


**Figure 1. Output threshold decrease reduces discriminability**
*A*, schematic representation of the model and quantification of discriminability. For each $k$, a set of binary inputs $\{X^{(i)}\}$ with the first set of $k$ active units (minimal overlapping activation) are considered more 'discriminable' if the pairwise distance (either with Jaccard distances $J_d$ or normalized Hamming distances $H_d$) of the corresponding outputs $\{Y^{(i)}\}$ is larger. $W$ is the weight matrix between $X$ and $Y$, $\theta$ is the output layer threshold while $\Delta\theta$ is the applied threshold change. *B*, illustration of the way $J_d$ (red) and $H_d$ (blue) change for specific pairs of outputs when $\Delta\theta$ changes the excitability of the outputs (green dots). *C* and *D*, the mean $J_d$ (red) and $H_d$ (blue) distances and mean output activity (black) are plotted as a function of $\Delta\theta$ for different $k$ (shadings) of $N_X = 10$ input units and different number of output units $N_Y$.

between these distances and threshold changes is shown in Fig. 1*C* and *D* for the optimized states.

Decreases in thresholds, for both cases, increase output activity as expected but decrease the binary distances $J_d$ and $H_d$, for different values of input pattern with minimal similarity $k$. As $k$ increases, the resulting output patterns become less distinguishable and $\Delta\theta < 0$ worsens the outcome. On the other hand, when $\Delta\theta > 0$, the effects still hold mainly for Jaccard distances, as they are more biased towards activated units. The dependence of the normalized Hamming distances on $\Delta\theta$ is non-monotonic (illustrated in Fig. 1*B*) as sparsification of output activity by a large threshold increase would eventually decrease pattern differences. Together, these considerations exemplify how detrimental it is for discrimination performance when output thresholds decrease.

## Single unit supra-threshold activation with incomplete patterns

A central hypothesis of this study is that, in contrast to pattern discrimination, the recognition of known but incomplete patterns may benefit from enhanced intrinsic excitability. To provide a proof-of-principle demonstration that a reduction in spike threshold enables neuronal activation with a lower number of synaptic inputs, we start with the simple example of a binary unit $Y$ activated by a Heaviside step function eqn (2). Its intrinsic excitability is characterized by the threshold of activation $\theta$. We assume that its activity represents the active state of all of its inputs in $X$ (Fig. 2). The connectivity $W$ from the input units in $X$ to the output of interest $Y$ could be generated in various ways. For simplicity, we choose to either draw them from a uniform distribution (eqn (1) and Fig. 2*A*) or assign equal values (Fig. 2*B*). For the former, on average, the weights would decrease linearly with their order (Fig. 2*C*). Either way, the weights are normalized to a sum of 1, for simplified control of the output threshold range.

When ignoring false positives (for now), an incomplete pattern in $X$ would be any pattern where at least one unit is inactive and the resulting active state of the output signifies the recognition of an input pattern despite such incompleteness. As shown in Fig. 2*A* and *B* (sub-panels *iv* and *v*), when there are not enough input units active or without the presence of high-weight inputs, low thresholds are required to evoke responses in the output unit. Although more inputs or the presence of stronger inputs would allow for more flexibility in the range of required thresholds (sub-panels *v*), in

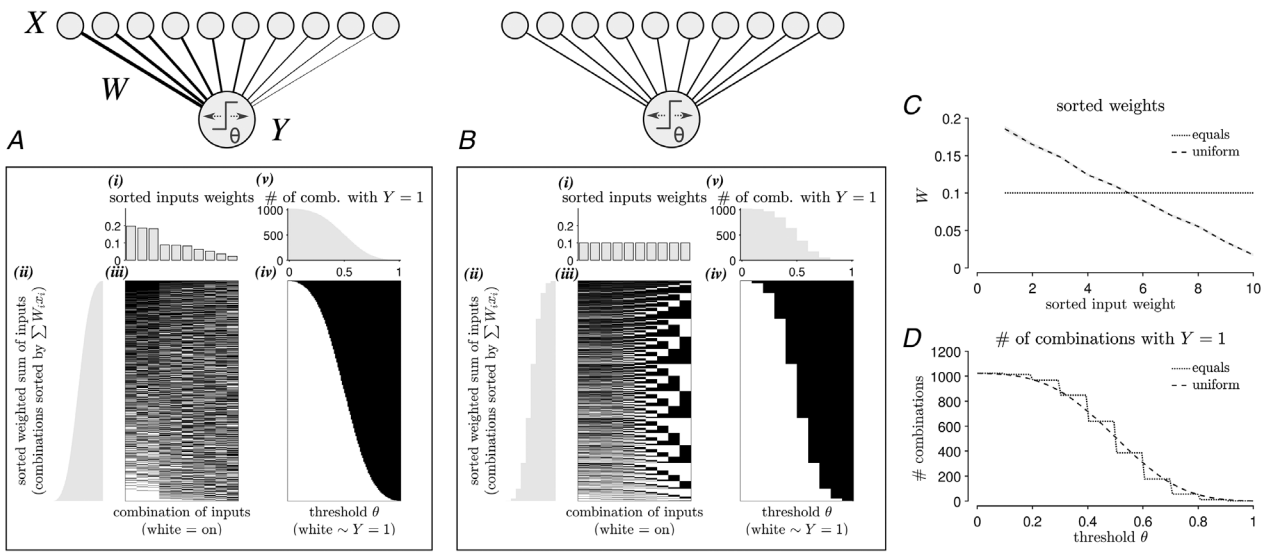


**Figure 2. Dependence of the number of input combinations resulting in supra-threshold activation ($N = 10$) on the threshold $\theta$**
Supra-threshold activation of the output $Y$ means that the weights sum of the inputs $X$ is greater than the threshold $\theta$, in other words $Y = 1$ if $\sum_i W_i x_i > \theta$. *A* and *B*, examples of the weights drawn from a uniform distribution (*A*) and when all are assigned the same value (*B*), respectively, before normalization to the sum. In each example panel: (*i*) shows the sorted input weights from $X \rightarrow Y$; (*ii*) shows the sorted weighted sum of the corresponding combination of the corresponding combinations of the inputs (*iii*); (*iv*) shows whether corresponding combinations in (*ii*, *iii*) would result in supra-threshold activation as a function of the threshold $\theta$ (*x*-axis); (*v*) indicates the number of combinations in (*iv*) showing supra-threshold activation, as a function of the threshold $\theta$ (*x*-axis). *C*, mean sorted weights for 50 instantiations for the equal-weight scenario (dotted line) and for the scenario where weights are initially drawn from a uniform distribution (dashed line). *D*, mean number of combinations resulting in supra-threshold activation, as a function of the threshold.

the absence of low thresholds the trade-off is that the number of patterns allowing for the recognition becomes limited, and that weaker inputs are likely insufficient. This might be problematic in cases where weak inputs convey information about relevant object details. A solution is lowering the threshold (sub-panels *ii* and *v*, Fig. 2*D*) of the output. In neural network terms, increased excitability, for example resulting from activity-dependent plasticity of membrane excitability, would allow for more patterns, even incomplete ones, to be sufficient to evoke supra-threshold responses regardless of the arrangement of input weights, e.g. few synaptic inputs with high input weights or more with low input weights.

This simple toy example hints at the possible computational benefit of intrinsic excitability when recognition is desired, but input components are missing. However, this example assumes that all inputs represent the object of interest, which is not the case when unnecessary inputs, or inputs belonging to another object (category) are present. Next, we are going to include irrelevant inputs to examine the possible problems and benefits for the recognition of the relevant input pattern.

## Recognition of known/learned patterns in a simple feedforward two-layer binary network

To extend the framework, we set up our model as a simple feedforward network with an input layer $X$ and an output layer $Y$, connected via the non-negative connectivity matrix $W_{YX}$ that describes the amount of selectivity of the inputs to each output unit via the selectivity index $W$ (selectivity of the output unit $Y$) and a specified amount of input overlap (overlap in pattern presentation in the input unit $X$) (eqn (7), Fig. 3*A* and *B*).

The (in)completeness of the inputs is characterized by the percentage complete parameter, with added noise. The output units at $Y$ are activated with a Heaviside step function (eqn 2), whose thresholds are characterized by the base thresholds $\theta_{\text{base}}$ and an additive threshold change $\Delta\theta$ in only one of the output units (Fig. 3*C*). $\Delta\theta < 0$ would be analogous to an increased intrinsic excitability of the affected artificial neuron compared to the other output units, whereas $\Delta\theta > 0$ would indicate decreased intrinsic excitability. Here, we look at the effects of $\Delta\theta$ on the performance in a recognition task (focus on the output whose threshold is changed) (Fig. 3*C*).

The results are shown in Fig. 4*A*, where recognition true positive rate (TPR) is shown in blue, while the tradeoff between TPR and the false-positive rate, FPR, (TPR − FPR) is shown in red. Because $N_Y = 3, \alpha_W < 1/3$ would be lower than chance, and thus highly undesirable for recognition. Increased selectivity emphasizes relevant inputs and reduces the weight of irrelevant ones, thus benefitting both performance parameters.

The dependence of recognition performance on $\Delta\theta$ (true positive rate; TPR) appears sigmoidal, inverted with the sign of threshold change (blue shaded lines in Fig. 4*A*). As expected, lowered thresholds allow for easier recognition of the output of interest, eventually reaching 100% TPR. When the selectivity index is high and the inputs are mostly complete, the unit does not require decreased thresholds to reach maximal recognition. However, for a given input completeness, weaker selectivity requires a more pronounced threshold decrease to reach a set performance level. The same is true when inputs become more incomplete, given a weak to moderate $\alpha_W$. Hence the optimal threshold change for maximal recognition leans toward stronger intrinsic potentiation $\Delta\theta < 0$ when either the inputs become more insufficient or the network selectivity strength $\alpha_W$ is imperfect (Fig. 4*C* and *D*).

Generally, FPR monotonically increases with decreases in threshold values. Overall, decreased input completeness leads to decreases of FPR as irrelevant inputs will have less of a chance to evoke responses in the relevant output unit Y. This would be more beneficial for recognition performance (see ROC curves in Fig. 4*B*).

As the goal is to maximize recognition performance without enhancing the false recognition rate, we want to maximize TPR while minimizing FPR, thus maximizing the difference TPR − FPR (red shaded lines in Fig. 4*A*). When selectivity is too low ($< 1/3$, leftmost top sub-panel in Fig. 4*A* and lightest grey line in the top right sub-panel in Fig. 4*D*), FPR is higher than TPR as irrelevant input strengths are now stronger than relevant connections, hence TPR − FPR $< 0$. In moderate selectivity strengths, these difference curves are negatively affected by increased input incompleteness and require more negative $\Delta\theta_{\text{optim}}$ to reach their maximum (Fig. 4*D*).

**Effects of input selectivity overlap.** Aside from the imperfection of selectivity ($\alpha_W < 1$), another possible issue that could arise intrinsically in the feedforward set-up is an overlap in input selectivity, as certain input units could activate more than one output. Here, we consider the worst case, in which some units connect strongly to all outputs (Fig. 3*B*). As we assume a fixed selective input number per output ($N_{\text{selec}} = 50$), non-zero overlap input units send relevant, but also irrelevant input to the output units. When selectivity strength is low, this reduces the relative contribution of relevant input.

As defined, recognition TPR is not really affected by the selectivity overlap, as we focus only on output units encoding the learned object pattern (Fig. 4*A*). This is because the high overlap allows the shared inputs to evoke responses in the affected output too easily when the input pattern actually belongs to another output class. For this reason, sparsity of input patterns is more

beneficial for the tradeoff between TPR and FPR (i.e. the difference) when $\Delta\theta < 0$. On the other hand, when $\Delta\theta > 0$, input completeness is better for the recognition tradeoff. However, if we look at the optimal threshold change, as input patterns become more incomplete and have a moderate selectivity index, $\Delta\theta_{\text{optim}}$ generally tends towards more negative changes in the case of non-zero selectivity overlap (Fig. 4*D*, bottom sub-panel).

A well-known analysis tool for examining binary classification performance is the ROC graph. As expected, increased input completeness would increase recognition performance Fig. 4*B*. Increase in selectivity overlap decreases the overall performance of the recognition task (compare top and bottom panels of Fig. 4*B*).

## Biological threshold potentials and activity-dependent plasticity

The purpose of re-analysing existing biological data sets is twofold. First, we would like to obtain information on the distribution of threshold values and the difference between resting and threshold potentials in cortex. Second, as our modelling has shown, negative changes in threshold potentials can signify a shift in neural

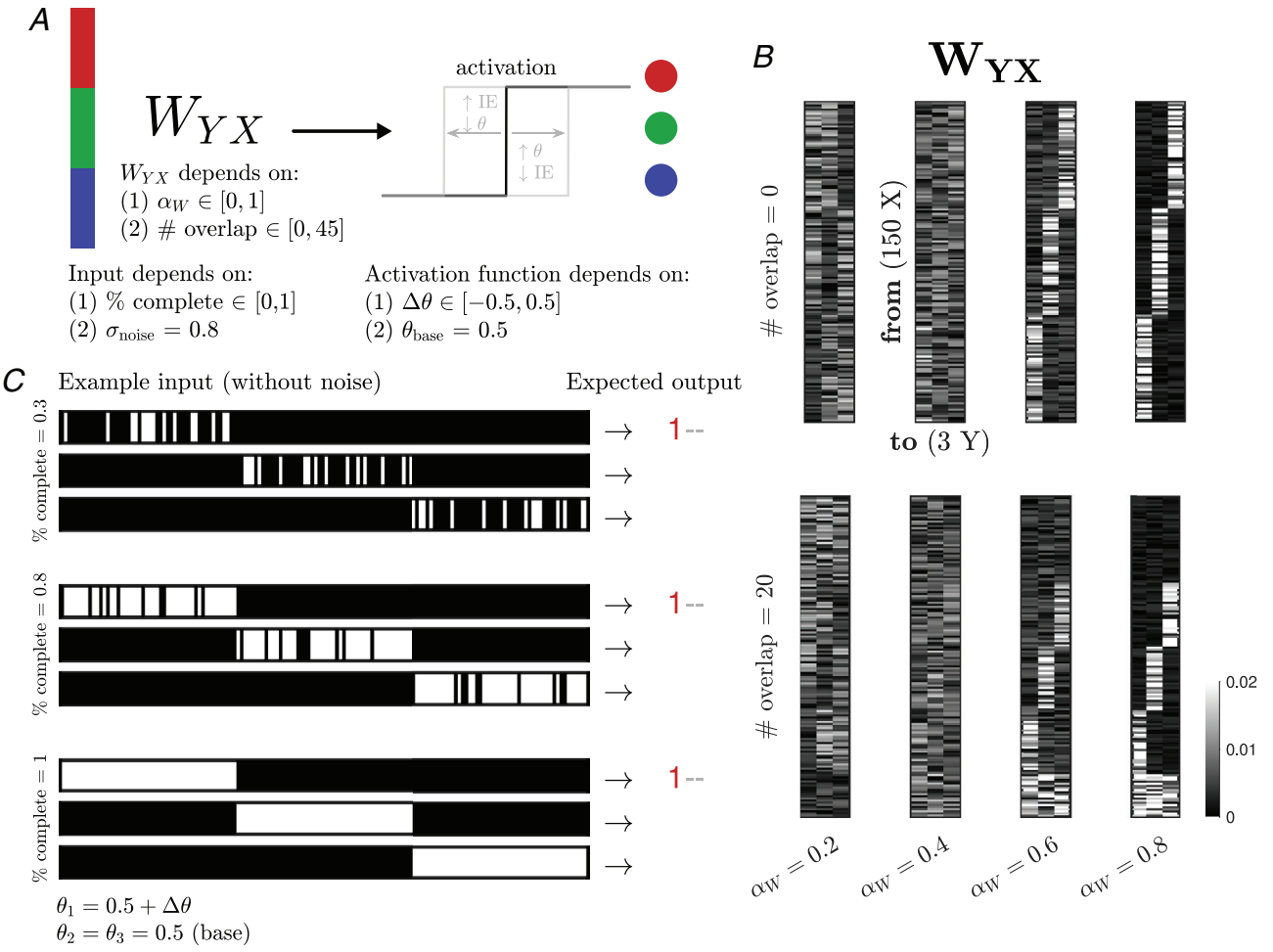


**Figure 3. Description of the abstract model with binary output units and the task of concern**
*A*, summary of model and task, and parameters involved. The model is a feedforward network comprised of an layer *X* (150 units in total) and output layer *Y* (3 units in total). The colors represent the selectivity for a specific output unit in each input unit. *B*, the excitatory connectivity matrix $W_{YX}$ is characterized by the selectivity index $\alpha_W$ and the number of overlap. Each sub-panel is an example with different pairs of ($\alpha_W$, # overlap). Higher $\alpha_W$ (from left to right) concentrates more input weights on the corresponding output that inputs are selective for. Higher number of overlap (top to bottom) creates more inputs selective for all output units, and simultaneously more inputs without any selectivity. *C*, the output activation function is a Heaviside-step function characterized by the constant base threshold ($\theta_{\text{base}}$ for all output units, and a certain threshold change $\Delta\theta$ for only one output unit (in this example the first output $Y_1$, colored red). The input patterns are parameterized by the '% complete' for each pattern – higher % complete (top to bottom) recruits more inputs. There is Gaussian noise added on top of the input patterns, with a fixed $\sigma_{\text{noise}}$ (not shown here for simplicity).

encoding strategies from accurate reporting of input patterns to interpretative reporting of whether a known or previously learned pattern is presented. In this latter scenario, it is of interest, which biological activity pattern drives this threshold adaptation and thus enables optimal signal processing when the history of the input pattern presentation (previously presented under favourable conditions or not) changes.

**Threshold potentials obtained from V1 *in vivo* recordings.** We obtained resting and threshold potentials from published whole-cell patch-clamp recordings from L2/3 pyramidal neurons in the primary visual cortex (V1) of awake macaque monkeys (Li et al., 2020). These recordings were performed in the laboratory of Dr Nicholas Priebe (University of Texas at Austin) and requested measures have been made available to us.

In this data set, resting potentials $V_R$ ranged from about −75 to −50 mV (−64.83 ± 6.39 mV, $n = 26$ cells from 3 animals) and threshold potentials $V_T$ ranged from about −60 to −40 mV (−51.48 ± 4.69 mV, $n = 26$). The difference between resting and threshold potentials $\Delta V_{TR}$ in these recordings (the distance in mV) ranged from 5 to 22 mV (13.34 ± 4.48 mV, $n = 26$) (Fig. 5). This analysis

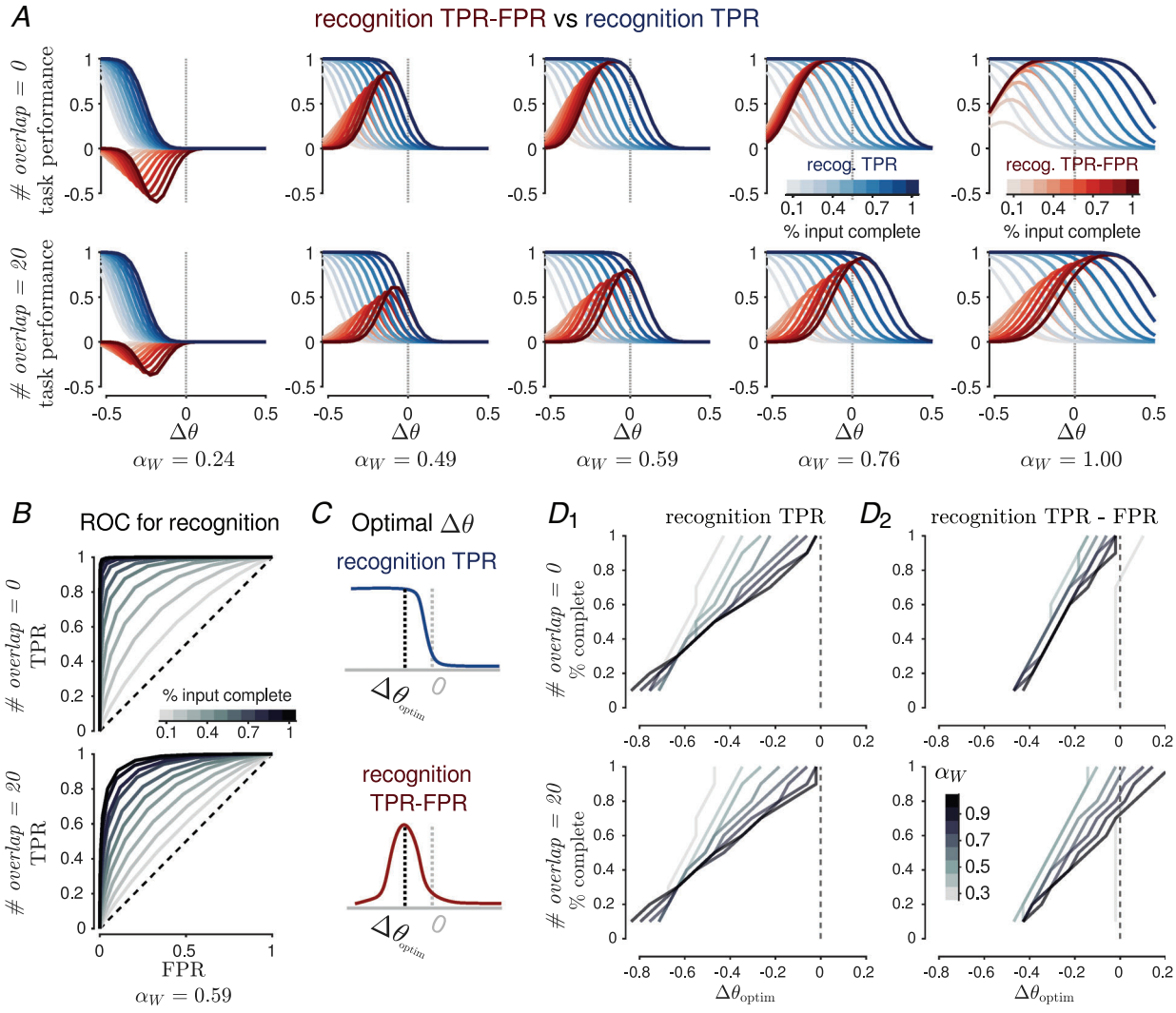


**Figure 4. Recognition performance based on the change of threshold in a single output unit**
*A*, the recognition trade off (TPR − FPR; shades of red) and recognition true-positive rate (TPR; shades of blue) as a function of threshold change ($\Delta\theta$). Increasing selectivity indices ($\alpha_W$) are shown from left to right. Two conditions of selectivity overlap are shown from top to bottom. Darker shades represent more complete patterns. *B*, receiver operating characteristics (ROC) of recognition with TPR and FPR plotted against each other with shadings indicating input completeness for $\alpha_W = 0.59$. *C*, demonstration of how $\Delta\theta_{optim}$ is obtained, as the threshold change with the smallest absolute value to achieve maximal performance. *D*, $\Delta\theta_{optim}$ of recognition TPR ($\mathbf{D}_1$) and tradeoff (TPR − FPR, $\mathbf{D}_2$) as a function of input completeness (*y*-axis) and selectivity set-up (strength/index: grey shading; overlap: top *vs*. bottom).

shows the range of threshold potentials assumed in a biological setting and under physiological conditions in the cortex of the awake macaque, an animal model that is as close as it gets to the human cortex.

**Threshold potentials and plasticity in S1 *in vitro* recordings.** Our own *in vitro* recordings from the primary sensory cortex (S1) of the mouse (Gill & Hansel, 2020) allow us to perform more detailed analyses, including the analysis of activity parameters that alter the threshold potential. The data are shown in Fig. 5*B*. We observe that the resting potentials $V_R$ in S1 assume values that are similar to those seen in the V1 cortex of awake macaques, roughly in the range of $-75$ to $-45$ mV (pre $= -65.50 \pm 5.25$ mV, post $= -65.73 \pm 6.72$ mV, paired pre *vs* post $t$-statistic $= 0.3807$, $P = 0.7063$, $n = 29$ cells). We did not observe significant differences between the resting potentials of S1 (combined pre and post) and V1 data ($t = -0.5433$, $P = 0.5884$). However, the threshold potentials $V_T$ occupy a more positive range than those observed in the V1 recordings; we observed a range from about $-50$ to $-30$ mV (pre $= -42.14 \pm 2.59$ mV, post $= -42.22 \pm 4.00$ mV, paired $t = 0.1311$, $P = 0.8966$, $n = 29$), as well as significant difference between S1 and V1 threshold potentials $V_T$ ($t = 10.3571$, $P = 1.4765 \times 10^{-16}$),

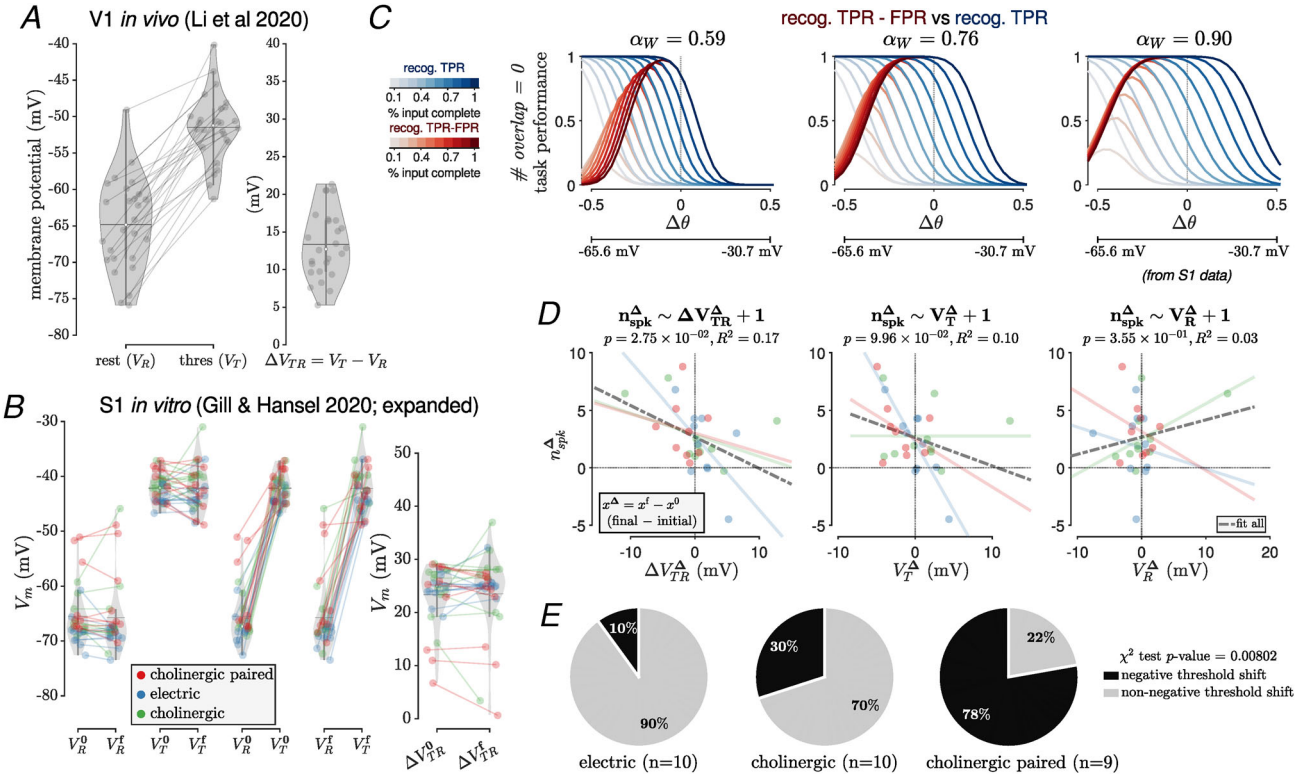


**Figure 5. Threshold potentials and plasticity: analysis of biological data sets**
*A*, biological data of neural spiking threshold ($V_T$), resting potentials ($V_R$) and their differences ($\Delta V_{TR} = V_T - V_R$) from *in vivo* V1 recordings obtained from Li et al. (2020). In each violin plot, horizontal lines show the mean, while white circles show the first quartile, median and third quartile from bottom to top. *B*, biological data of $V_T$, $V_R$ and $\Delta V_{TR}$ from *in vitro* data taken from (Gill & Hansel, 2020) and new recordings at initial values ($V^0$) and after plasticity induction ($V^f$). Colours indicate different plasticity induction protocols: electrical activation (somatic depolarization or synaptic activation) in blue; cholinergic group using oxo-m bath application in green; and cholinergic paired with electrical activation (somatic depolarization) in red. *C*, the recognition tradeoff (shades of red) and recognition true-positive rate (shades of blue) as a function of threshold change ($\Delta\theta$) for three conditions of selectivity indices ($\alpha_W$) are shown as an example of the model calculations to compare with the lower and upper threshold potential bounds measured in mouse S1 cortex. The lower bound is the average of resting potentials ($n = 29$), while the upper bound is the average of threshold potentials during the relative refractory period calculated from a new data set ($n = 4$). *D*, relationship between functional change (number of spikes $n_{spk}$) and membrane potential change ($V_R$, $V_T$, $\Delta V_{TR}$) after induction protocols are applied (colour legends are same as in *B*). Change is denoted as $x^{\Delta} = x^f - x^0$, as the difference between initial and final values of variable $x$. Colored lines are linear fits using data from each induction group, while dashed grey lines are linear fits using all the data. *E*, distribution of S1 recordings from the three different experimental groups according to category membership, based on $\Delta V^{\Delta}_{TR}$, to either 'negative threshold shift' or 'non-negative threshold shift'.

leading to a larger difference between resting and threshold potentials ($\Delta V_{TR}$) in S1 than in V1 (V1 $= 13.34 \pm 4.48$ mV, S1 pre $= 23.36 \pm 5.70$ mV, S1 post $= 23.51 \pm 7.80$ mV; V1 *vs* S1 two-sample $t = 6.9342$, $P = 8.6032 \times 10^{-10}$). A caveat of our V1 to S1 comparisons certainly is that the values were taken from different recording conditions (*in vivo* for V1, *in vitro* – without an attempt to 'activate' the slice – for S1). Note, however, that the finding of a larger $\Delta V_{TR}$ corresponds to observations made in S1 cortex of intact rats (Brecht et al., 2003).

The *in vivo* V1 data set (Li et al., 2020) from the Priebe laboratory does not contain plasticity data, but our own published recordings from L2/3 pyramidal neurons in S1 mouse cortex *in vitro* do (Gill & Hansel, 2020). As reported in Gill & Hansel (2020), three manipulations lead to increases in the measure of excitability used in this work, the number of spikes evoked by somatic injection of a depolarizing current test pulse. In a total of 29 recordings (23 from that study and 6 additional recordings), the experimental manipulations and number of recorded cells per manipulation are as follows: electric activation (repeated injection of depolarizing currents or tetanic activation of excitatory synapses; $n = 10$); bath application of the muscarinic agonist oxo-m (7 $\mu$M; $n = 10$); and paired oxo-m application with electric stimulation ($n = 9$). All three protocols cause an increase in excitability (Gill & Hansel, 2020) and therefore qualify as efficient IP protocols Fig. 5*D*. Changes in threshold potential have not been analysed and reported in Gill & Hansel (2020), but are examined here.

Significant negative threshold changes $V_T$ were observed with paired electric and cholinergic activation ($-1.96 \pm 2.37$ mV, paired Student's $t$-statistic $= 2.4897$, $P = 0.0375$, $n = 9$), but not with electric ($0.23 \pm 2.28$ mV, $t = -0.3210$, $P = 0.7555$, $n = 10$) or cholinergic activation alone ($1.29 \pm 4.76$ mV, $t = -0.8549$, $P = 0.4148$, $n = 10$). Thus, cholinergic co-activation provides the most efficient means to trigger a lowering of the spike threshold.

We cannot fit the thresholds observed directly to our model shown in Fig. 4*A*, but made an attempt to approximate minimal and maximal threshold potential values that correspond to the $-0.5$ and 0.5 edges of the model plots. As the spike threshold $V_T$ cannot be lower than the resting potential $V_R$, we accepted the average resting potential measured in our recordings as an approximation of $\theta_{min} = 0$, $\Delta\theta_{min} = -0.5$. The value obtained from our recordings ($n = 29$) is $-65.61$ mV (combined pre and post measurements).

As the theoretically available most positive threshold bound $\theta_{max} = 1$, $\Delta\theta_{max} = 0.5$, we accepted the membrane potential at which action potentials are evoked from a depolarizing pulse when the neuron is in a (relative) refractory state. In a set of new recordings, this value was determined to be $-30.71$ mV ($n = 4$; Fig. 5*C*). Therefore, the threshold shifts available for optimization of performance in the recognition task are limited to a maximal range of about 35 mV. Note that in our set of 29 recordings, the range of 'real' (measured in the non-refractory state) threshold potentials ($V_T$) was about $10 - 15$ mV wide. Although this observation does not exclude the possibility that larger changes can take place, in particular with repeated instead of single activation periods, it seems likely (and plausible) that under physiological conditions the range of assumed threshold potentials is smaller than the theoretically available one.

How does this threshold potential influence the spike output in our recordings? First, we notice that threshold plasticity ($V_T^\Delta$, $\Delta V_{TR}^\Delta$) is bidirectional, even though the change in spike number ($n_{spk}^\Delta$) is largely unidirectional. This means that in some cells the threshold for spike firing is enhanced, but once passed, more spikes can be evoked. Second, this bidirectional change leads to a widening of the range of threshold potentials after IP is triggered (Fig. 5*B*). Additionally, we observe significant negative association between the changes in spike number ($n_{spk}^\Delta$) and threshold-to-rest distance changes ($\Delta V_{TR}^\Delta$) ($rho = -0.41$, $R^2 = 0.17$, $P = 0.0275$), but not with the changes of the other two membrane potential variables ($P = 0.0996$ for $V_T^\Delta$ and $P = 0.3547$ for $V_R^\Delta$). This observation does not imply that $V_T$ and $V_R$ have no impact on spike firing. What it shows is that – as can be predicted from the definition of $\Delta V_{TR}$ as the actual membrane potential difference that has to be overcome to reach threshold – spike firing is most sensitive to changes in $\Delta V_{TR}$.

Our model on the relationship between performance in a recognition task and changes in the threshold potential suggests that under a wide range of conditions task performance benefits from a reduction in the spike threshold distance, $\Delta V_{TR}$. The experimental data presented in Gill & Hansel (2020) allow us to examine what type of neuronal activation causes a negative $\Delta V_{TR}$ shift and therefore alter the neuron's coding strategy to one that favours the recognition of known/learned input patterns, in particular when the presented pattern is incomplete. To assess differences in the efficacy to promote negative threshold changes, we applied a $\chi^2$ test of independence for the distribution of threshold potential changes triggered by the three types of manipulations used (electric, cholinergic and cholinergic paired with electric), along two categories: negative and non-negative threshold changes. Here, the category 'negative threshold change' includes all threshold distance changes, i.e. $\Delta V_{TR}^\Delta$ in a negative direction regardless of amplitude. We defined two exceptions: (a) the negative threshold change category does not include recordings, in which there was a decrease in spike number that might offset

some effects of the threshold change, and (b) cells with a 'null' direction change in threshold potential were counted as 'non-negative'. Based on the distribution of threshold changes, we identified four recordings, in which these potential values clustered around zero change, and whose percentual change remained $< 1\%$. We therefore defined a negative threshold change as one exceeding the 1% threshold distance. With this definition of categories, in 7/9 recordings with paired cholinergic and electric activation a negative threshold change was observed, while this was only the case in 3/10 recordings in which cholinergic activation was applied alone, and in 1/10 recordings in which electric activation was applied alone (Fig. 5*E*). The paired cholinergic activation was the only activation pattern to promote a significant negative threshold change ($\chi^2 = 9.6504$; $P = 0.00802$).

## Discussion

The first main finding from our study is that intrinsic plasticity benefits and enables neural coding strategies that aim at the recognition of known, but incompletely presented input patterns. This interpretative coding comes at the expense of coding precision; this effect is a direct consequence of the loss of resolution that results from the fact that intrinsic amplification applies to all synaptic inputs located 'upstream' of where the excitability is changed. As such, this phenomenon is not restricted to near-somatic changes in spike threshold, but will equally apply to excitability changes specific to dendritic compartments (Losonczy et al., 2008; Ohtsuki et al., 2012).

The second main finding is that a shift in coding mode is promoted by electrical activity paired with cholinergic signalling, but not by electric or cholinergic activation alone (Alejandre-Garcıá et al., 2022; note that threshold changes can generally also be triggered in the absence of cholinergic agonists; e.g. Paz et al., 2009). In contrast, under our experimental conditions – which may provide a less efficient drive for plasticity – cholinergic co-activation emerges as a factor that facilitates this aspect of intrinsic plasticity. This observation is of interest, because of what the coding modes imply. High-accuracy representation and encoding of input patterns is advantageous when unknown patterns need to be distinguished. It is not known what the pattern should look like, so an incomplete pattern cannot be distinguished from the complete, unknown pattern. Interpretative encoding, in contrast, matches a pattern against a known pattern, and reports whether the presented pattern belongs to an expected category or matches a specific object of interest. The finding that this shift in encoding strategy results from paired cholinergic and electric activation is of interest, as this activation configuration can be expected to create – via learning – known patterns out of previously unknown ones upon repeated presentation and with a certain level of attention. Our identification of cholinergic co-activation as a critical contributor to IP does not exclude other, additional mechanisms. For example, it has been shown that IP in cortical pyramidal neurons is triggered by the activation of metabotropic glutamate receptors (mGluRs) that regulate small-conductance, calcium-dependent SK-type $K^+$ channels (Sourdet et al., 2003). Together with our study on mAChR-mediated regulation of SK channels (Gill & Hansel, 2020), this observation assigns a critical role in excitability control and plasticity to $G_{aq}$-coupled metabotropic receptors that downregulate SK conductances. Other neuromodulator receptors, e.g. serotonergic 5-HT receptors (e.g. Celada et al., 2013), are present as well, but a direct contribution to intrinsic plasticity in neocortical pyramidal cells has not been demonstrated yet. The cellular machinery is present to allow for excitability alterations by a variety of mechanisms. *In vivo* recordings from cortical pyramidal neurons confirm that the ultimate control of bidirectional IP and threshold plasticity is executed by ion channels that can indeed affect excitability parameters, namely primarily $Na^+$ and/or $K^+$ conductances (Mahon & Charpier, 2012). $I_h$ current generally is a candidate contributor to intrinsic plasticity as well, but is only expressed at low levels in L2/3 pyramidal cells (Larkum et al., 2007) and was therefore not investigated further.

In an initial step, we demonstrate that increased excitability, in the form of a reduction in threshold potential, harms output discrimination. This is because intrinsic excitability amplifies responsiveness of $>1$ synaptic input, which results in enhanced 'merging' of output patterns, and a reduction in the resolution of object/pattern representation. A related phenomenon is known from pattern separation in granule cells of the hippocampal dentate gyrus: in temporal lobe epilepsy, granule cells may downregulate their excitability, in effect restoring hampered pattern separation (Yim et al., 2015). In contrast, performance in a recognition task does improve with reduced spike thresholds, in particular under conditions that are challenging for perception, such as a low degree of input selectivity in the output cells $Y$ and/or the presentation of incomplete patterns. The latter observation is a positive consequence of the unspecific nature of amplification: a reduction in the spike threshold will allow a higher number of input combinations (synapses) to evoke spike firing. To stay in our example of neurons specialized in face recognition, successful detection of a face (as an object category) or successful detection of a specific, individual face becomes possible even when details of the object are missing or only details are presented. Such flexibility in input detection is one of the requirements for the detection of known objects, which points to an essential nature of intrinsic plasticity mechanisms in neuronal encoding

strategies. In expansion of such a role, it has been observed that neurons fire at similar rates for pairs of objects for which an associative relationship has been learned, while they fire at different rates for pairs of objects that have no learned association (Freedman & Assad, 2011). This finding suggests that membrane excitability, in addition to shared synaptic drive, can become a signature of encoded objects that the network groups into object categories. Synaptic connectivity remains an important factor, and therefore it is noteworthy that a similar amplification would result from an increase of weights across all excitatory synapses. The reason why biological networks do not seem to use this synaptic strategy is possibly that such upregulation would depend on the activity of all synapses. It would be nearly impossible to do so without changing synaptic weight ratios, with unforeseeable consequences for object representation.

The improvement in performance of the recognition task upon lowering of the spike threshold is limited by the fact that false-positives emerge next to true-positives. The FPR rate will increase alongside the TPR rate when intrinsic amplification rises, and thus the probability of incorrect object identification (false recognition) increases as well. The difference between these detection rates, TPR − FPR, depends on the selectivity index $\alpha_W$ (TPR − FPR increases with high selectivity values), the degree of input overlap (it increases with low overlap) and pattern completeness (it increases with a high degree of completeness). The dependence on these parameters allows us to determine optimal spike thresholds for different parameter constellations, with maximal relative changes of −0.4 to −0.5 being required under non-preferential detection conditions. While the occurrence of false positives cancels out some of the advantages of intrinsic plasticity in the recognition of objects, it is possible that biological networks may compensate for this effect by identifying false positives via network effects. In this scenario, individual neurons may signal positive recognition at short delays (and this coding would be reflected in the TPR rate), while computations within the larger network would enable correction for false positives; in such cases, the TPR rate would actually better reflect performance than the TPR − FPR difference.

## Reference to biological excitability data

We have analysed data sets obtained from whole-cell patch-clamp recordings from L2/3 pyramidal cells in V1 cortex of awake macaques (Li et al., 2020) and in S1 cortex of mice *in vitro* (Gill & Hansel, 2020). These data sets make it possible to assess the range of assumed thresholds under awake conditions (macaques) and the plasticity range under *in vitro* conditions (mice). The recordings from cortical slices that are used here include activation protocols that trigger intrinsic plasticity. Our analysis shows that in V1 cortex the threshold is up to about 20 mV more positive than the resting potential. In S1 cortex, the distance is somewhat higher, up to about 30 mV. This difference in $\Delta V_{TR}$ might well be partially related to the species and experimental conditions. However, unlike the primary somatosensory cortex (Brecht et al., 2003), visual cortices are known to operate in a 'high-input regime' that is signified by strong synaptic input and high-frequency spike activity at rest (Shadlen & Newsome, 1998). It therefore is possible that these different types of neurons adjust their spike thresholds differently to optimize their firing properties for different neural coding goals.

We find that all three activation patterns – electric, cholinergic and paired – all tend to increase excitability as measured by the number of evoked spikes. In contrast, the threshold potential is bidirectionally changed over a total range of about 10 mV. Negative threshold changes are preferentially initiated by paired electric and cholinergic activation (Fig. 5*D* and *E*). As the spike threshold is the only excitability parameter that is informative about spiking *versus* non-spiking conditions, the threshold is critical in determining a neuron's ability to participate in any neuronal ensemble.

## Realistic constraints for abstract model variables

The hyperparameters used (selectivity strength, overlap and input incompleteness) are somewhat abstract and do not in themselves carry information about relevant parameter ranges. Therefore, we offer below some additional notes and predictions on values that these hyperparameters may realistically assume.

First, imperfect *selectivity strength* ($\alpha_W < 1$) is typically expected in realistic settings as individual neurons are known to respond to considerable input variance. While the realistic range of $\alpha_W$ values is difficult to determine, we can make some simple predictions regarding the relationship between selectivity strength and intrinsic excitability. Increased object familiarity, via repeated presentation of a certain input, would allow $\alpha_W$ to increase. In fact, repeated synaptic activity, which conveys the information that an input pattern is repeatedly or persistently present, may lead to co-occurring synaptic and intrinsic potentiation (e.g. Belmeguenai et al., 2010). This is meaningful as $\alpha_W$ is likely to stay $< 1$ (a value of 1 would be equivalent to the presence of only one input, albeit potentially represented by multiple synapses). Our model shows that $\alpha_W$, over a wide range of assumed values $< 1$, makes it necessary to reduce threshold to maximize task performance. Thus, the co-occurrence of synaptic potentiation with enhanced excitability has the capacity to move both parameters into an optimal parameter space.

Second, non-zero *selectivity overlap* in lower layers of encoding is expected in biological systems, especially for

distributed coding of complex objects. Such objects often are composed of building blocks that are on their own similar between otherwise different objects, as much as a Lego figure is different from any other, but the individual Lego pieces are the same. A biological example is a face that is entirely unique, even though specific components, such as eye colour, only exist in a limited number of variations. This phenomenon causes overlap as eyes are a common input component to encode for faces; even with consideration of eye colours, the same eye colour might be shared between otherwise different faces. The presence of overlap is not always a limiting factor. For instance, it could allow for (a) reinforced recognition, especially in weak input conditions, or (b) contribution of encoding object co-occurrence for higher-order concepts. However, at the same time, high selectivity overlap often poses a challenge for differentiation (in discrimination and recognition tasks), which generally is made easier the more object components differ.

Third, while selectivity overlap is a potential intrinsic network concern and is sometimes difficult to quantify, *input incompleteness* (or sparsity) is intuitively relevant as a concern in real-world settings. How much this parameter matters for recognition, we argue, depends on the 'need' (goal) for such recognition task, which might further constrain the optimal excitability states. For example, engrams responsible for predator detection might benefit from higher excitability with some leeway on false positives (for a field mouse, recognition of a predator by only a few simple features, such as recognition of a bird of prey by its silhouette, enhances the probability of survival). In face recognition cells in primates, which may recognize an individual in a position-independent manner, input completeness is expected to always be $< 1$, because the object can only be presented in one position at a time, leaving the other possible object constellations unrepresented. Such parameter constraints determine critical ranges for optimal threshold values that our model describes.

### Hints from artificial settings in machine learning

Machine learning algorithms show astounding analogies to IP. For example, batch-normalization (BN) is a form of input normalization that is applied during the training of deep learning models. Though the exact mechanism is still debated, BN is known to speed up training and to smooth the optimization landscape (Ioffe & Szegedy, 2015; Santurkar et al., 2019); in addition, it serves as a form of regularization during training (Luo et al., 2019). A recent study (Shaw et al., 2020) points out (a) the similarity between neural IP and machine learning BN as both perform certain transformations of the inputs with adaptive parameters based on the history of the input statistics, and (b) that their implementation speeds up training in image classification tasks trained on multi-layer-perceptron and convolutional networks. Interestingly, another study (Frankle et al., 2021) shows that deep artificial neural networks trained solely using BN parameters could reach non-trivial classification performance. Combining both of these recent works, one could hypothesize that if synaptic weights of a neural network are frozen or the weight learning rate is much slower than the intrinsic update (which is biologically plausible, for example Lopez-Rojas et al. (2016) shows dendritic IP is more easily inducible than SP), appropriate changes to the parameters characterizing the artificial non-linearity could achieve significant improvement with fewer adaptive parameters. In other words, given a 'status-quo' network topology, training only the intrinsic parameters to adapt artificial single unit non-linearity might achieve better performance in an energy efficient manner, which is advantageous when it is expensive to change the synaptic profiles of the network (Gallistel, 2017). In both biological and machine learning scenarios, it appears that IP enables a shift from faithful/accurate to interpretative decoding, which may be an essential coding strategy in fast-changing environments where some object features remain hidden, but objects nevertheless need to be swiftly recognized, or at least categorized.

The work presented here highlights the role that threshold plasticity in particular plays in this adaptation of coding strategy. It further shows that cholinergic co-activation, a cellular modulation mechanism associated with attention and thus detection of signal salience, promotes the adaptation step. Thus, neuromodulation-inspired features of deep neural networks (Mei et al., 2022) may include consequences of IP, in particular threshold plasticity. As we have shown here, this phenomenon promotes the recognition of incomplete objects and assignment to object categories.

## References

Alejandre-Garcıá, T., Kim, S., Pérez-Ortega, J., & Yuste, R. (2022). Intrinsic excitability mechanisms of neuronal ensemble formation. *eLife*, **11**, e77470.

Baek, E., Das, N. R., Cannistraci, C. V., Rim, T., Bermúdez, G. S. C., Nych, K., Cho, H., Kim, K., Baek, C.-K., Makarov, D., Tetzlaff, R., Chua, L., Baraban, L., & Cuniberti, G. (2020). Intrinsic plasticity of silicon nanowire neurotransistors for dynamic memory and learning functions. *Nature Electronics*, **3**(7), 398–408.

Belmeguenai, A., Hosy, E., Bengtsson, F., Pedroarena, C. M., Piochon, C., Teuling, E., He, Q., Ohtsuki, G., De Jeu, M. T. G., Elgersma, Y., De Zeeuw, C. I., Jörntell, H., & Hansel, C. (2010). Intrinsic plasticity complements long-term potentiation in parallel fiber input gain control in cerebellar purkinje cells. *Journal of Neuroscience*, **30**(41), 13630–13643.

Bliss, T. V., & Lomo, T. (1973). Long-lasting potentiation of synaptic transmission in the dentate area of the anaesthetized rabbit following stimulation of the perforant path. *Journal of Physiology*, **232**(2), 331–356.

Brecht, M., Roth, A., & Sakmann, B. (2003). Dynamic receptive fields of reconstructed pyramidal cells in layers 3 and 2 of rat somatosensory barrel cortex. *Journal of Physiology*, **553**(1), 243–265.

Celada, P., Puig, M. V., & Artigas, F. (2013). Serotonin modulation of cortical neurons and networks. *Frontiers in Integrative Neuroscience*, **7**, 25.

Dalgaty, T., Payvand, M., Moro, F., Ly, D. R. B., Pebay-Peyroula, F., Casas, J., Indiveri, G., & Vianello, E. (2019). Hybrid neuromorphic circuits exploiting non-conventional properties of RRAM for massively parallel local plasticity mechanisms. *APL Materials*, **7**(8), 081125.

Del Papa, B., Priesemann, V., & Triesch, J. (2019). Fading memory, plasticity, and criticality in recurrent networks. In N. Tomen, J. M. Herrmann, & U. Ernst (Eds.), *The functional role of critical dynamics in neural systems* (pp. 95–115). Cham: Springer International Publishing.

Felleman, D. J., & Van Essen, D. C. (1991). Distributed hierarchical processing in the primate cerebral cortex. *Cerebral Cortex*, **1**(1), 1–47.

Frankle, J., Schwab, D. J., & Morcos, A. S. (2021). Training BatchNorm and only BatchNorm: On the expressive power of random features in CNNs. *arXiv:200300152 [cs, stat]*. http://arxiv.org/abs/2003.00152.

Freedman, D. J., & Assad, J. A. (2011). A proposed common neural mechanism for categorization and perceptual decisions. *Nature Neuroscience*, **14**(2), 143–146.

Gallistel, C. R. (2017). The coding question. *Trends in Cognitive Sciences*, **21**(7), 498–508.

Gallistel, C. R., & Balsam, P. D. (2014). Time to rethink the neural mechanisms of learning and memory. *Neurobiology of Learning and Memory*, **108**: 136–144.

Gallistel, C. R., & Matzel, L. D. (2013). The neuroscience of learning: Beyond the hebbian synapse. *Annual Review of Psychology*, **64**(1), 169–200.

Gershman, S. J., Balbi, P. E., Gallistel, C. R., & Gunawardena, J. (2021). Reconsidering the evidence for learning in single cells. *eLife*, **10**, e61907.

Gill, D. F., & Hansel, C. (2020). Muscarinic modulation of SK2-Type k+ channels promotes intrinsic plasticity in L2/3 pyramidal neurons of the mouse primary somatosensory cortex. *eNeuro*, **7**(2), ENEURO.0453-19.2020.

Hansel, C., & Disterhoft, J. F. (2020). Why is synaptic plasticity not enough? *Neurobiology of Learning and Memory*, **176**: 107336.

Hansel, C., Linden, D. J., & D'Angelo, E. (2001). Beyond parallel fiber LTD: The diversity of synaptic and non-synaptic plasticity in the cerebellum. *Nature Neuroscience*, **4**(5), 467–475.

Hopfield, J. J. (1982). Neural networks and physical systems with emergent collective computational abilities. *Proceedings of the National Academy of Sciences, USA*, **79**(8), 2554–2558.

Innocenti, G. M. (1981). Growth and reshaping of axons in the establishment of visual callosal connections. *Science*, **212**(4496), 824–827.

Innocenti, G. M. (1995). Exuberant development of connections, and its possible permissive role in cortical evolution. *Trends in Neuroscience*, **18**(9), 397–402.

Ioffe, S., & Szegedy, C. (2015). Batch normalization: Accelerating deep network training by reducing internal covariate shift. In: *Proceedings of the 32nd international conference on international conference on machine learning, volume* **37**. Lille, France: , p. 448–456.

Izhikevich, E. M., & Edelman, G. M. (2008). Large-scale model of mammalian thalamocortical systems. *Proceedings of the National Academy of Sciences, USA*, **105**(9), 3593–3598.

Johansson, F. (2019). Intrinsic memory of temporal intervals in cerebellar purkinje cells. *Neurobiology of Learning and Memory*, **166**: 107103.

Johansson, F., Carlsson, H. A. E., Rasmussen, A., Yeo, C. H., & Hesslow, G. (2015). Activation of a temporal memory in purkinje cells by the mGluR7 receptor. *Cell reports*, **13**(9), 1741–1746.

Joshi, P., & Triesch, J. (2009). Rules for information maximization in spiking neurons using intrinsic plasticity. In: *2009 international joint conference on neural networks*. Atlanta, GA, USA: IEEE. p. 1456–1461.

Josselyn, S. A., & Tonegawa, S. (2020). Memory engrams: Recalling the past and imagining the future. *Science*, **367**(6473), eaaw4325.

Larkum, M. E., Waters, J., Sakmann, B., & Helmchen, F. (2007). Dendritic spikes in apical dendrites of neocortical layer 2/3 pyramidal neurons. *Journal of Neuroscience*, **27**(34), 8999–9008.

Lazar, A., Pipa, G., & Triesch, J. (2007). Fading memory and time series prediction in recurrent networks with different forms of plasticity. *Neural Networks*, **20**(3), 312–322.

LeMasson, G., Marder, E., & Abbott, L. F. (1993). Activity-dependent regulation of conductances in model neurons. *Science*, **259**(5103), 1915–1917.

Li, B., Routh, B. N., Johnston, D., Seidemann, E., & Priebe, N. J. (2020). Voltage-Gated intrinsic conductances shape the Input-Output relationship of cortical neurons in behaving primate V1. *Neuron*, **107**(1), 185–196.e4.

Li, C., & Li, Y. (2016). A review on synergistic learning. *IEEE Access*, **4**, 119–134.

Li, X., Wang, W., Xue, F., & Song, Y. (2018). Computational modeling of spiking neural network with learning rules from STDP and intrinsic plasticity. *Physica A: Statistical Mechanics and its Applications*, **491**: 716–728.

Li, Y., & Li, C. (2013). Synergies between intrinsic and synaptic plasticity based on information theoretic learning. *Plos One*, **8**(5), e62894.

Loidolt, M., Rudelt, L., & Priesemann, V. (2020). Sequence memory in recurrent neuronal network can develop without structured input. *bioRxiv*. https://doi.org/10.1101/2020.09.15.297580.

Lopez-Rojas, J., Heine, M., & Kreutz, M. R. (2016). Plasticity of intrinsic excitability in mature granule cells of the dentate gyrus. *Science Reports*, **6**(1), 21615.

Losonczy, A., Makara, J. K., & Magee, J. C. (2008). Compartmentalized dendritic plasticity and input feature storage in neurons. *Nature*, **452**(7186), 436–441.

Luo, P., Wang, X., Shao, W., & Peng, Z. (2019). Towards understanding regularization in batch normalization. *arXiv:180900846 [cs, stat]*. http://arxiv.org/abs/1809.00846 [18 Nov. 2021].

Mahon, S., & Charpier, S. (2012). Bidirectional plasticity of intrinsic excitability controls sensory inputs efficiency in layer 5 barrel cortex neurons in vivo. *Journal of Neuroscience*, **32**(33), 11377–11389. https://doi.org/10.1523/JNEUROSCI.0415-12.2012.

Marder, E., Abbott, L. F., Turrigiano, G. G., Liu, Z., & Golowasch, J. (1996). Memory from the dynamics of intrinsic membrane currents. *Proceedings of the National Academy of Sciences, USA*, **93**(24), 13481–13486.

Marder, E., & Prinz, A. A. (2002). Modeling stability in neuron and network function: The role of activity in homeostasis. *Bioessays*, **24**(12), 1145–1154.

McCormick, D. A., & Prince, D. A. (1985). Two types of muscarinic response to acetylcholine in mammalian cortical neurons. *Proceedings of the National Academy of Sciences, USA*, **82**(18), 6344–6348.

Mei, J., Muller, E., & Ramaswamy, S. (2022). Informing deep neural networks by multiscale principles of neuromodulatory systems. *Trends in Neuroscience*, **45**(3), 237–250.

Moyer, J. R. Jr, Thompson, L. T., & Disterhoft, J. F. (1996). Trace eyeblink conditioning increases CA1 excitability in a transient and learning-specific manner. *Journal of Neuroscience*, **16**(17), 5536–5546.

Nabavi, S., Fox, R., Proulx, C. D., Lin, J. Y., Tsien, R. Y., & Malinow, R. (2014). Engineering a memory with LTD and LTP. *Nature*, **511**(7509), 348–352.

Naude, J., Cessac, B., Berry, H., & Delord, B. (2013). Effects of cellular homeostatic intrinsic plasticity on dynamical and computational properties of biological recurrent neural networks. *Journal of Neuroscience*, **33**(38), 15032–15043.

Ohtsuki, G., Piochon, C., Adelman, J. P., & Hansel, C. (2012). SK2 channel modulation contributes to compartment-specific dendritic plasticity in cerebellar purkinje cells. *Neuron*, **75**(1), 108–120.

Paz, J. T., Mahon, S., Tiret, P., Genet, S., Delord, B., & Charpier, S. (2009). Multiple forms of activity-dependent intrinsic plasticity in layer V cortical neurones in vivo. *Journal of Physiology*, **587**(13), 3189–3205.

Popescu, I. R., Le, K. Q., Ducote, A. L., Li, J. E., Leland, A. E., & Mostany, R. (2021). Increased intrinsic excitability and decreased synaptic inhibition in aged somatosensory cortex pyramidal neurons. *Neurobiology of Aging*, **98**, 88–98.

Santurkar, S., Tsipras, D., Ilyas, A., & Madry, A. (2019). How does batch normalization help optimization? *arXiv:180511604 [cs, stat]*. http://arxiv.org/abs/1805.11604 [18 Nov. 2021].

Savin, C., Joshi, P., & Triesch, J. (2010). Independent component analysis in spiking neurons. *PLoS Computational Biology*, **6**(4), e1000757.

Schreurs, B. G., Gusev, P. A., Tomsic, D., Alkon, D. L., & Shi, T. (1998). Intracellular correlates of acquisition and long-term memory of classical conditioning in purkinje cell dendrites in slices of rabbit cerebellar lobule HVI. *Journal of Neuroscience*, **18**(14), 5498–5507.

Shadlen, M. N., & Newsome, W. T. (1998). The variable discharge of cortical neurons: Implications for connectivity, computation, and information coding. *Journal of Neuroscience*, **18**(10), 3870–3896.

Shaw, N. P., Jackson, T., & Orchard, J. (2020). Biological batch normalisation: How intrinsic plasticity improves learning in deep neural networks. *PLoS One*, **15**(9), e0238454.

Singer, W. (1995). Development and plasticity of cortical processing architectures. *Science*, **270**(5237), 758–764.

Sivagnanam, S., Majumdar, A., Yoshimoto, K., Astakhov, V., Anita, B., Martone, M., & Carnevale, N. T. (2013). Introducing the neuroscience gateway. *CEUR Workshop Proceedings*, **993**.

Sourdet, V., Russier, M., Daoudal, G., Ankri, N., & Debanne, D. (2003). Long-term enhancement of neuronal excitability and temporal fidelity mediated by metabotropic glutamate receptor subtype 5. *Journal of Neuroscience*, **23**(32), 10238–10248.

Steil, J. J. (2007). Online reservoir adaptation by intrinsic plasticity for backpropagation-decorrelation and echo state learning. *Neural Networks*, **20**(3), 353–364.

Stemmler, M., & Koch, C. (1999). How voltage-dependent conductances can adapt to maximize the information encoded by neuronal firing rate. *Nature Neuroscience*, **2**(6), 521–527.

Titley, H. K., Brunel, N., & Hansel, C. (2017). Toward a neurocentric view of learning. *Neuron*, **95**(1), 19–32.

Titley, H. K., Watkins, G. V., Lin, C., Weiss, C., McCarthy, M., Disterhoft, J. F., & Hansel, C. (2020). Intrinsic excitability increase in cerebellar purkinje cells after delay Eye-Blink conditioning in mice. *Journal of Neuroscience*, **40**(10), 2038–2046.

Triesch, J. (2005). A gradient rule for the plasticity of a neuron's intrinsic excitability. In: *Artificial neural networks: Biological inspirations – ICANN 2005*. Springer Berlin Heidelberg, p. 65–70.

Triesch, J. (2007). Synergies between intrinsic and synaptic plasticity mechanisms. *Neural Computation*, **19**(4), 885–909.

Turrigiano, G. G. (1999). Homeostatic plasticity in neuronal networks: The more things change, the more they stay the same. *Trends in Neuroscience*, **22**(5), 221–227.

Wang, X., Jin, Y., & Hao, K. (2020). Synergies between synaptic and intrinsic plasticity in echo state networks. *Neurocomputing*, **432**, 32–43. https://doi.org/10.1016/j.neucom.2020.12.007.

Wu, Y. K., Hengen, K. B., Turrigiano, G. G., & Gjorgjieva, J. (2020). Homeostatic mechanisms regulate distinct aspects of cortical circuit dynamics. *Proceedings of the National Academy of Sciences, USA*, **117**(39), 24514–24525.

Yamasaki, M., Matsui, M., & Watanabe, M. (2010). Preferential localization of muscarinic M1 receptor on dendritic shaft and spine of cortical pyramidal cells and its anatomical evidence for volume transmission. *Journal of Neuroscience*, **30**(12), 4408–4418.

Yim, M. Y., Hanuschkin, A., & Wolfart, J. (2015). Intrinsic rescaling of granule cells restores pattern separation ability of a dentate gyrus network model during epileptic hyperexcitability. *Hippocampus*, **25**(3), 297–308.

Zhang, A., Zhou, H., Li, X., & Zhu, W. (2019). Fast and robust learning in spiking Feed-Forward neural networks based on intrinsic plasticity mechanism. *Neurocomputing*, **365**, 102–112.
Zhang, W., & Li, P. (2019). Information-Theoretic intrinsic plasticity for online unsupervised learning in spiking neural networks. *Frontiers in Neuroscience*, **13**, 31.
Zheng, P., & Triesch, J. (2014). Robust development of synfire chains from multiple plasticity mechanisms. *Frontiers in Computational Neuroscience*, **8**, 66.

## Additional information

### Data availability statement

The code will be at https://github.com/HAN-CELL-LAB/PhamHansel-intrinsic-exc-2022. The *in vitro* S1 data have been collected in the Hansel laboratory (Gill & Hansel, 2020) and will be made available online at the same URL address. The *in vivo* V1 data are obtained from Dr Nicholas J. Priebe (Li et al., 2020). All experimental data and all essential modelling data are included in the manuscript figures.

### Competing interests

The authors have no conflicts of interest to declare.

### Author contributions

The work was performed in the Hansel laboratory at the University of Chicago, IL, USA. C.H. contributed to the conception of the work. T.P. and C. H. contributed to the design of the work. T.P. contributed to the acquisition and analysis of the data. C.H. contributed to the interpretation of the data. T.P. and C. H. contributed to the drafting of the manuscript. Both authors approved the final version of the manuscript, and agree to be accountable for all aspects of the work in ensuring that questions related to the accuracy or integrity of any part of the work are appropriately investigated and resolved. All persons designated as authors qualify for authorship, and all those who qualify for authorship are listed.

### Funding

This work was funded by the National Institute of Neurological Disorders and Stroke (NINDS): NINDS-NS62771.

### Acknowledgements

The authors thank Dr Nicholas J. Priebe (University of Texas, Austin) for providing us with the *in vivo* V1 data (Li et al., 2020). The authors thank Drs Yali Amit, Brent Doiron and Stephanie Palmer (University of Chicago) for their feedback on the manuscript. We are grateful to Silas E. Busch for help with patch-clamp recordings from mouse S1 cortex.

### Keywords

cholinergic, intrinsic plasticity, pattern recognition, pyramidal neuron, spike threshold

## Supporting information

Additional supporting information can be found online in the Supporting Information section at the end of the HTML view of the article. Supporting information files available:

**Statistical Summary Document**
**Peer Review History**